Stabilization of Protein by Replacement of a Fluctuating Loop: Structural Analysis of a Chimera of Bovine α-Lactalbumin and Equine Lysozyme†

Masahito Tada,‡ Yoshihiro Kobashigawa,§ Mineyuki Mizuguchi,‡ Kazunori Miura,‡,|| Takahide Kouno,‡ Yasuhiro Kumaki,⊥ Makoto Demura,§ Katsutoshi Nitta,§ and Keiichi Kawano*,‡

Faculty of Pharmaceutical Sciences, Toyama Medical and Pharmaceutical University, Toyama, Japan, Division of Biological Sciences, Graduate School of Science, Hokkaido University, Sapporo, Japan, and High Resolution NMR Laboratory, Graduate School of Science, Hokkaido University, Sapporo, Japan

Received May 15, 2002

ABSTRACT: Equine lysozyme is a calcium-binding lysozyme and an evolutional intermediate between non-calcium binding c-type lysozyme and α-lactalbumin. We constructed a chimeric protein by substituting the fluctuating loop of bovine α-lactalbumin with the D-helix of equine lysozyme. The substitution affects the protection factors not only in the fluctuating loop but also in the antiparallel *β*-sheet, the A- and B-helices, and the loop between the B-helix and the *β*-sheet. Amide protons in these regions of the chimera are more protected from exchange than are those of bovine α-lactalbumin. We used model-free analysis based on ^{15}N nuclear magnetic resonance relaxation measurements to investigate the dynamics of the main chain of the chimera and showed that the fluctuating loop of the chimera is as rigid as three major helices. When we analyzed the chemical shift deviations and backbone HN−H$^{\alpha}$ scalar coupling constants, we found that the chimera showed an α-helical tendency in residues around the fluctuating loop. Our results suggest that the replacement of a highly fluctuating loop in a protein with a rigid structural element in a homologous one may be useful to stabilize the protein structure.

α-Lactalbumin (α-LA) is a mammalian Ca^{2+}-binding protein that plays an important role in the biosynthesis of lactose. The attachment of α-LA to *β*-galactosyl transferase results in a complex, lactose synthetase, which catalyzes the production of lactose from UDP-galactose and glucose (*1*, *2*). On the other hand, c-type lysozyme is a ubiquitous lytic enzyme that degrades the peptidoglycan of bacterial cell walls. The two functions are quite different, but α-LA and c-type lysozyme are homologous proteins that are presumed to have diverged from a common ancestor because of similarities in primary structure, gene sequence, and three-dimensional structure (*3*−*6*). While most lysozymes cannot bind Ca^{2+}, equine lysozyme (ELZ) binds Ca^{2+} tightly and is considered to be an intermediate in the molecular evolution from non-Ca^{2+}-binding lysozyme to α-LA (*7*, *8*).

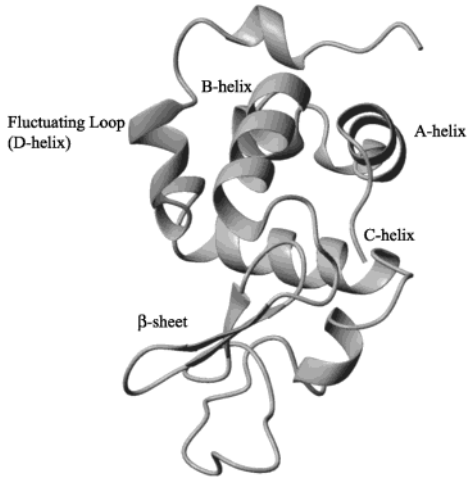

FIGURE 1: Three-dimensional structure of bovine α-lactalbumin [PDB code 1HFZ, (*10*)]. The figure was generated using the program MOLMOL (*45*).

X-ray crystallographic studies have shown that the three-dimensional structures of α-LA and c-type lysozyme are similar to each other (*5*, *6*). Both proteins are small globular proteins comprised of two types of subdomains, i.e., the α- and *β*-subdomains (*5*, *9*). The α-subdomain contains four α-helices (A to D), and the *β*-subdomain has a three-stranded antiparallel *β*-sheet (Figure 1). The conformation in residues 105−110 of α-LA is particularly interesting, since this region of α-LA adopts a variety of distinct conformations. Residues 105−110 show a distorted α-helical conformation (D-helix)

† This work was supported by Grant-in-Aid for Scientific Research from the Ministry of Education, Culture, Sports, Science and Technology of Japan and the Program for the Promotion of Basic Research Activities for Innovative Biosciences (Japan).

* Corresponding author. Address: Faculty of Pharmaceutical Sciences, Toyama Medical and Pharmaceutical University, 2630 Sugitani, Toyama 930-0194, Japan. Tel: 81-76-434-5061. Fax: 81-76-434-5061. E-mail: kawano@ms.toyama-mpu.ac.jp.

‡ Toyama Medical and Pharmaceutical University.

§ Division of Biological Sciences, Graduate School of Science, Hokkaido University.

|| Present address: Structural Biology Group, Research Institute of Biological Resources, National Institute of Advanced Industrial Science and Technology (AIST), 2-17-2-1 Tsukisamu-Higashi, Toyohira, Sapporo 062-8517, Japan.

⊥ High Resolution NMR Laboratory, Graduate School of Science, Hokkaido University.

[1] Abbreviations: α-LA, α-lactalbumin; ELZ, equine lysozyme; HPLC, high-performance liquid chromatography; NMR, nuclear magnetic resonance; DSS, 4,4-dimethyl-4-silapentane-1-sulfonic acid; DSC, differential scanning calorimetry; DQF-COSY, double quantum filtered correlation spectroscopy; TOCSY, total correlation spectroscopy; NOESY, nuclear Overhauser effect spectroscopy; HSQC, heteronuclear single quantum coherence; 3D, three-dimensional; 2D, two-dimensional.

10.1021/bi020360u CCC: $22.00
Published on Web 10/26/2002

Table 1: Amino Acid Sequences of Equine Lysozyme (ELZ), Bovine α-Lactalbumin (α-LA), and Chimeric Protein (BLAELZ)[a]

												D-Helix						
ELZ	D	P	K	G	M	S	A	W	**K^{109}**	**A**	**W**	**V**	**K**	**H^{114}**	C	K	D	K
Bovine α-LA	D	K	V	G	I	N	Y	W	**L^{105}**	**A**	**H**	**K**	**A**	**L^{110}**	C	S	E	K
BLAELZ	D	K	V	G	I	N	Y	W	**K^{105}**	**A**	**W**	**V**	**K**	**H^{110}**	C	S	E	K
												Fluctuating Loop (D-Helix)						

[a] The residues of the D-helix and fluctuating loop are shown in bold type.

in bovine α-LA, whereas it adopts a loop structure in goat and guinea-pig α-LA (*10*). In human α-LA, both structures are observed in the residues 104−111 at different pH values and temperatures. However, it has been shown that the crystals of both forms appear at pH 6.5 and room temperature, suggesting the highly fluctuating structure in the Trp104-Cys111 region (*11*). Nuclear magnetic resonance (NMR) studies of bovine, human, and guinea pig α-LA have shown that peaks for residues in the 105−110 region are either broadened or absent from ^{1}H−^{15}N heteronuclear single quantum coherence (HSQC) spectra (*12*). This observation suggests the conformational exchange on a millisecond to microsecond time scale. Therefore, the D-helix (residues 105−110) of α-LA is referred to as a fluctuating loop. In contrast, the corresponding region (residues 109−114; D-helix) in c-type lysozyme forms a rigid α-helix (*6*, *13*, *14*). Furthermore, the amide-hydrogen exchange studies of c-type lysozymes indicated that the amide protons of the D-helix exchange slowly in contrast to the rapid amide hydrogen exchange in the fluctuating loop of α-LA (*12*, *15*−*18*). We therefore considered it intriguing to investigate how insertion of the D-helix of c-type lysozyme into α-LA would affect the structure and stability of α-LA (*19*). In the present study, we investigated the structure and stability of a chimera, BLAELZ, in which the amino acid sequence of the fluctuating loop (residues 105−110) comes from equine lysozyme and the remainder of the sequence comes from bovine α-LA (Table 1).

EXPERIMENTAL PROCEDURES

Production of the Chimera. Mutations were made as described previously (*20*) and were verified by sequencing the entire mutated genes. The chimeric protein was expressed and purified as described previously (*21*). In short, the chimeric protein was expressed in *Escherichia coli* BL21 (DE3) as inclusion bodies. Uniformly ^{15}N-labeled protein was obtained by growing the cells in M9 medium containing $^{15}NH_4Cl$ as a sole nitrogen source. Cells were lysed by sonication, and the insoluble fraction was solubilized in 8 M urea and then loaded onto a DEAE-Sepharose column. The column was eluted with a linear gradient of NaCl in the presence of 6 M urea. The partially purified protein was diluted and oxidatively refolded by dialyzing the protein solution against a refolding buffer without urea. The oxidized protein was purified by reverse-phase high-performance liquid chromatography (HPLC).

NMR Spectroscopy. NMR spectra were acquired at 20 °C on JEOL α-500 and Bruker DMX500 spectrometers. Sample solutions for multi-dimensional NMR were obtained by dissolving BLAELZ in 90% H_2O/10% D_2O. The protein concentration was 1−1.5 mM, the pH was adjusted to 6.3, and $CaCl_2$ was added, bringing the concentration to 2 mM. Conventional two-dimensional (2D) NMR spectra, i.e., double quantum filtered correlation spectroscopy (DQF-COSY) (*22*), total correlation spectroscopy (TOCSY) (*23*, *24*), nuclear Overhauser effect spectroscopy (NOESY) (*25*, *26*), and conventional ^{15}N-edited spectra, i.e., ^{1}H−^{15}N HSQC (*27*), ^{1}H−^{15}N TOCSY-HSQC, ^{1}H−^{15}N NOESY-HSQC (*28*), and HNHA (*29*), were acquired. All ^{15}N-edited spectra were gradient-enhanced. The NOESY and TOCSY mixing times for all measurements were set at 100−200 and 80 ms, respectively. Sweep widths of 8000 Hz were used for the ^{1}H and 1800 Hz for the ^{15}N dimensions, with the carrier frequency set at the water resonance (4.687 ppm). Data sets for ^{15}N-edited TOCSY and NOESY experiments were typically composed of 512 (^{1}H) × 128 (^{1}H) × 64 (^{15}N) of 16 or 8 scans. Data sets for 2D DQF-COSY, TOCSY, and NOESY experiments were typically composed of 1024 (^{1}H) × 512 (^{1}H) of 32 to 64 scans, and for HSQC the data sets were composed of 1024 (^{1}H) × 512 (^{15}N) of 32 scans, with a sweep width of 8000 Hz for the ^{1}H and 3600 Hz for the ^{15}N dimensions. All proton chemical shifts were referenced to methyl resonance of 4,4-dimethyl-4-silapentane-1-sulfonic acid (DSS), used as an internal standard. The ^{15}N chemical shift was indirectly referenced by using the ratios 0.101 to ^{1}H of the zero-point frequencies. Data processing was performed on a Silicon Graphics Indy work station using the program packages NMR Pipe (*30*) and XEASY (*31*).

Hydrogen/Deuterium Exchange. The hydrogen exchange rate measurements of BLAELZ were carried out using a 0.6 mM sample of uniformly ^{15}N-labeled BLAELZ. The exchange was initiated by dissolving lyophilized protein in 280 μL of D_2O d_4−acetate buffer containing 2 mM $CaCl_2$ at a direct pH meter reading of 6.3. HSQC spectra were collected at 500 MHz at 20 °C every 3 h for 3 days. Data sets of all NMR spectra for hydrogen exchange measurements were composed of 512 (^{1}H) × 128 (^{15}N) of 32 scans and a sweep width of 8000 Hz for the ^{1}H and 1800 Hz for the ^{15}N dimensions. The hydrogen exchange rates were determined as described previously (*12*).

^{15}N NMR Relaxation Measurements. Measurements of the longitudinal (T_1) and transverse (T_2) relaxation times and the heteronuclear nuclear Overhauser effects (NOEs) of ^{15}N nuclei were carried out as described previously (*32*). All spectra were processed and analyzed using NMR Pipe (*30*) and PIPP (*33*). The peak intensities of each cross-peak in a series of 2D NMR data were extracted using NMR Pipe based on the peak position defined by the contour averaging algorithm with the program PIPP. A series of extracted intensity profiles of each cross-peak was used for the calculation of the T_1 and T_2 relaxation times, using a single-exponential model function. The steady-state ^{1}H−^{15}N NOE values were determined from the ratios of the intensities of the peaks with and without proton saturation.

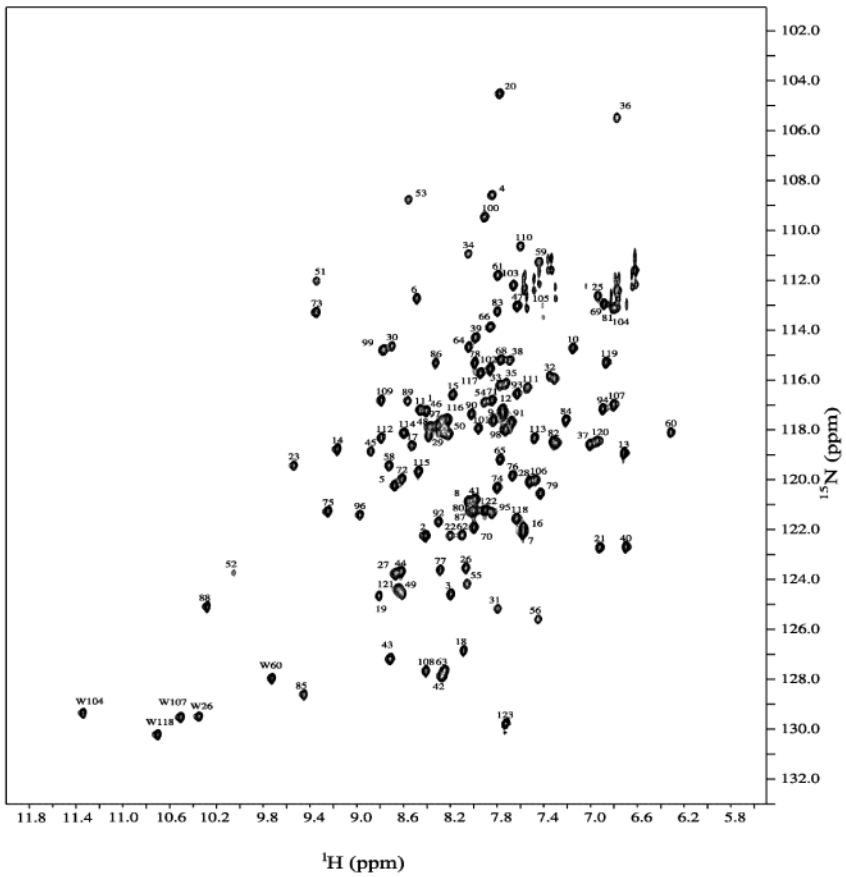

FIGURE 2: HSQC spectrum of BLAELZ at pH 6.3 and 20 °C, including backbone assignments. Assignments of the backbone resonances for most residues are indicated in the figure; others are omitted for clarity. The indole amide protons of tryptophan residues are indicated by W.

Model-Free Analysis. Model-free parameters were obtained using the FORTRAN program Modelfree (provided by A. G. Palmer) according to the protocol described by Palmer et al. (*34*). The optimization of the overall rotational correlation time, τ_m, was repeated until it came to the convergence (*35*).

Differential Scanning Calorimetry. Differential scanning calorimetry (DSC) measurements were carried out on a MC-2 microcalorimeter (MicroCal, Inc., Northampton, MA) at a scan rate of 1.0 K/min. The protein concentrations for DSC measurements were 92−136 μM. Buffer solutions contained 10 mM borate buffer (pH 8.0), 50 mM NaCl, and 1 mM $CaCl_2$. Unfolding temperature (T_m), calorimetric enthalpy (ΔH_{cal}), and van't Hoff enthalpy (ΔH_{vH}) were determined from the DSC curves using Origin software (MicroCal, Inc.).

RESULTS

NMR Assignments of the Chimeric Protein. The ^{1}H−^{15}N HSQC spectrum of BLAELZ at 20 °C is shown in Figure 2. The resonances are well dispersed, showing that BLAELZ has well-defined tertiary structure. Backbone ^{1}H and ^{15}N resonances of 120 of the 123 residues were assigned sequence-specifically by analyzing three-dimensional (3D) ^{1}H−^{15}N NOESY-HSQC and ^{1}H−^{15}N TOCSY-HSQC spectra. Gradient-enhanced 3D TOCSY-HSQC and NOESY-HSQC spectra provided the necessary through-bond and through-space correlations respectively (*36*−*38*). Backbone $^{1}H^{\alpha}$, ^{1}HN, and ^{15}N chemical shifts of BLAELZ were in excellent agreement with those of bovine α-LA in a previous study except for some residues, including those near the fluctuating loop (*12*). This indicates that the overall structure of BLAELZ is similar to that of bovine α-LA.

Table 2: Exchange Rate Constants of Trp Indole $N^{\epsilon 1}$ Protons of BLAELZ and ELZ

BLAELZ[a]		ELZ[b]	
	k_{ex}[c]		k_{ex}[c]
Trp26	1.1×10^{-3}	Trp28	1.4×10^{-7}
Trp104	6.5×10^{-6}	Trp108	1.0×10^{-6}
Trp107	3.3×10^{-6}	Trp111	1.4×10^{-5}

[a] pH 6.3, 20 °C (from this study). [b] pH 4.5, 25 °C [from ref *16*]. [c] In s^{-1}.

Amide Hydrogen Exchange of the Chimeric Protein. We measured the rates of solvent exchange of amide hydrogen atoms in the native state of BLAELZ by recording ^{1}H−^{15}N HSQC spectra as a function of time following dissolution of the protein in D_2O at pH 6.3 and 20 °C. Exchange rates were determined for 71 amide hydrogen atoms of the protein main-chain and for the side-chain indole hydrogen of Trp26, Tpr104, and Trp107. The other amide protons exchanged too rapidly to be monitored. To compare the hydrogen exchange properties of BLAELZ with those of bovine α-LA and ELZ, the protection factor ($P = k_{int}/k_{ex}$), defined as the ratio of the exchange rates experimentally determined and intrinsic for the amide proton (*39*), was determined for individual amide protons as described previously (*12*).

As has been observed previously for bovine and human α-LAs and ELZ, the residues with highly protected amide

Table 3: Coupling Constants $^3J_{HN,H\alpha}$ and Chemical Shift Index Analysis of BLAELZ[a]

No.	1									10									20									30									40
A. A.	E	Q	L	T	K	C	E	V	F	R	E	L	K	D	L	K	G	Y	G	G	V	S	L	P	E	W	V	C	T	T	F	H	T	S	G	Y	D	T	Q	A
CSI	β	β	β	β	α	c	α	α	α	α	α	c	α	α	c	α	β	α		β	α	c	β		α	c	α	α	β	α	α	α	α	c	α	α	c	α	β	α
$^3J_{HN,H\alpha}$		c	c	c		α		α		c	α		α	α			c	α		c	β		α		α	α		α		α		c		β		α	β			α
						A-helix												**3_{10}**							**B-helix**															

No.										50									60									70									80
A. A.	I	V	Q	N	N	D	S	T	E	Y	G	L	F	Q	I	N	N	K	I	W	C	K	D	D	Q	N	P	H	S	S	N	I	C	N	I	S	C	D	K	F
CSI	β	β	β	β	c	c	β		β	α	β		α	α	α	c	β	c	β	α	β	β	c	α	α	β		β	β	α	α	α	α	α	β	β	β	α	α	β
$^3J_{HN,H\alpha}$		c	β				c						.	β			α		β	α	c	β			α	c							α	β		c	c		α	α	
		β-sheet					**β-sheet**							**β-sheet**																												

No.										90									100									110									120
A. A.	L	D	D	D	L	T	D	D	I	M	C	V	K	K	I	L	D	K	V	G	I	N	Y	W	K	A	W	V	K	H	C	S	E	K	L	D	Q	W	L	C
CSI	β	β	c	β	β	α	α	c		α	β	α	α	α	α	α	α	β	β	β	β	α	α	β	β		α		α	β	β	β	β	α	β	α	α	c	β	α
$^3J_{HN,H\alpha}$		α		β	β	α					c	α	α	α		α	α					α				c	α	α	α				c	c		α	c	c			
												C-helix																			**Fluctuating loop**										**3_{10}**			

No.			
A. A.	E	K	L
CSI	β	c	c
$^3J_{HN,H\alpha}$		β	β

[a] Coupling constants $^3J_{HN,H\alpha}$ are represented by characters: α, $^3J_{HN,H\alpha} \leq 6.0$ [Hz]; c, $6.0 < {}^3J_{HN,H\alpha} < 8.0$ [Hz]; and *β*, $^3J_{HN,H\alpha} \geq 8.0$ [Hz]. In CSI analysis: α, chemical shift difference ≤ -0.1 [ppm]; c, $-0.1 <$ chemical shift difference < 0.1 [ppm]; *β*, chemical shift difference ≥ 0.1 [ppm]. A blank means that the signal was not detected or could not be analyzed.

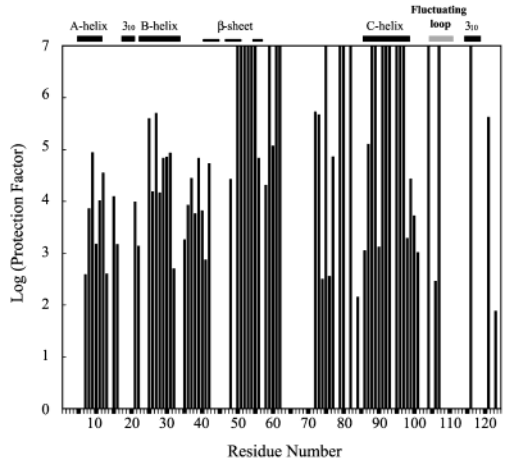

FIGURE 3: Protection factor versus amino acid residue number. Locations secondary structure elements are indicated in the figure.

protons are observed in both the α- and *β*-domains of BLAELZ (Figure 3). In the α-domain of BLAELZ, high protection against hydrogen exchange is observed for amide protons in the A- and B-helices. Amide protons in the C-helix exhibit much higher protection factors compared with those in the rest of the α-domain of BLAELZ. This pattern is somewhat similar to that observed for bovine α-LA in a previous study (*12*). As has been observed previously for bovine α-LA, no protection is observed in residues 63−71 of BLAELZ.

There are significant differences in the hydrogen exchange protection exhibited by BLAELZ and bovine α-LA (Figure 3). High protection from hydrogen exchange was observed in the fluctuating loop of BLAELZ; residues Ala106 and Trp107 are significantly protected from exchange. No protection was observed in the fluctuating loop of bovine α-LA (*12*). Highest protection (log $P > 7$) is observed at the Trp104 residue just proximal to the fluctuating loop (Figure 3); the protection factor of Trp104 in bovine α-LA is less than 10^5 (*12*).

The rate constants for Trp indole $N^{\epsilon 1}$ protons are shown in Table 2. High protection from hydrogen exchange is observed for the $N^{\epsilon 1}$ protons of three Trp residues, Trp26, 104, and 107 in BLAELZ. The $N^{\epsilon 1}$ protons of the other two residues, Trp60 and 118, exchange too rapidly to be used as probes.

Chemical Shifts and Backbone $^3J_{HN,H\alpha}$ Coupling Constants. The chemical shift deviations from random coil values (*40*) are shown in Table 3. The chemical shift deviations were obtained by subtraction of random coil values from $^1H^\alpha$ resonances of BLAELZ. We analyzed the $^1H^\alpha$ chemical shifts of 115 out of 123 residues. Another index of backbone secondary structure, $HN-H^\alpha$ scalar coupling constants (*29*), $^3J_{HN,H\alpha}$, is also shown in Table 3. We also analyzed the $^3J_{HN,H\alpha}$ coupling constants of 62 out of 123 residues. The chemical shift deviations and $^3J_{HN,H\alpha}$ coupling constants are represented by the characters α, *β*, and c (α, α-helical tendency; *β*, *β*-sheet tendency; and c, disordered tendency). In the fluctuating loop, three residues, Val108, Lys109, and His110, show an α-helical tendency in $^3J_{HN,H\alpha}$ coupling constants. Trp107 and Lys109 represent an α-helical tendency in the chemical shift deviations.

Polypeptide Chain Dynamics of BLAELZ. Relaxation rates measured for the ^{15}N nuclei were used to obtain insights into the dynamics of the polypeptide backbone of BLAELZ. The relaxation rates R_1 ($=1/T_1$) and R_2 ($=1/T_2$) and the heteronuclear $^1H-^{15}N$ NOE were measured for the cross-peaks in the $^1H-^{15}N$ HSQC spectra. To investigate the dynamics of

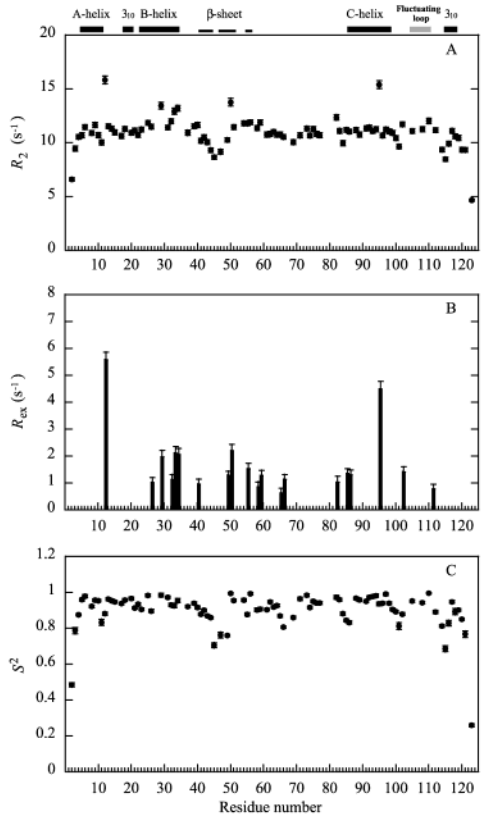

FIGURE 4: ^{15}N relaxation data and model-free parameters for BLAELZ. (A) A plot of the relaxation rate R_2 ($=1/T_2$) against residue number. (B and C) The R_{ex} and S^2 values calculated from T_1, T_2, and NOE are plotted against amino acid residue numbers.

Table 4: Thermodynamic Parameters for the Unfolding of Bovine α-LA and BLAELZ in 10 mM Borate Buffer (pH 8.0), 50 mM NaCl, and 1 mM $CaCl_2$

	Bovine α-LA	BLAELZ
T_m (°C)	59.19	64.13
ΔH_{cal} (kcal mol^{-1})	57.8 ± 0.27	65.8 ± 0.19
ΔH_{vH} (kcal mol^{-1})	66.2 ± 0.38	70.8 ± 0.26

the polypeptide chain, model-free analysis was performed for 89 out of 123 residues as described previously (*35*). The overall rotational correlation time, τ_m, was estimated to be 8.39 ± 0.012 ns.

The R_2 values, the chemical exchange term, R_{ex}, and order parameters, S^2, derived from the analysis of the relaxation data are shown in Figure 4 (*35*). There is no significant R_{ex} term around the fluctuating loop (Lys105 to His110). The S^2 values are greater than 0.8 for the majority of residues. The N and C termini show substantially lower order parameters than do other region of the protein. Low order parameters ($S^2 < 0.8$) were observed for the residues Asn45, Ser47, Glu49, and Leu115, indicating the high mobility of the backbone on a picosecond to nanosecond time scale (*35*).

Differential Scanning Calorimetry of BLAELZ. We investigated the thermal stability of BLAELZ using DSC and compared it with that of bovine α-LA. Unfolding temperature, calorimetric enthalpy, and van't Hoff enthalpy are summarized in Table 4. These unfolding parameters of bovine α-LA are similar to those reported previously (*41*). The T_m value of BLAELZ is higher than that of bovine α-LA, indicating that the thermal stability of BLAELZ is higher than that of bovine α-LA (Table 4).

DISCUSSION

Slow rates of amide hydrogen exchange are associated with shielding of amide protons from solvent, and slow exchanges most commonly result from hydrogen bonding interactions of the amide protons. The hydrogen exchange behavior of both bovine and human α-LA in the native state has been reported previously and has shown that no protection from exchange is observed for residues in the fluctuating loop of α-LA (*12*, *17*). Our present results show that the substitution of the fluctuating loop in bovine α-LA with the D-helix in ELZ affects the hydrogen exchange behavior of α-LA in the fluctuating loop (Figure 3). The backbone amide protons of Trp104, Ala106, and Trp107 of BLAELZ are significantly protected from exchange, indicating the presence of structure around the fluctuating loop of BLAELZ (Figure 3). Ala106 and Trp107 are located in the fluctuating loop, and Trp104 is just proximal to the fluctuating loop (Table 1). High protection from exchange in the fluctuating loop of BLAELZ is similar to that observed in the D-helix of ELZ (*15*, *16*).

There are other significant differences in the hydrogen exchange protection exhibited by BLAELZ in this report and bovine α-LA in a previous study (*12*). For instance, although no protection is observed around the C-terminal 3_{10} helix in the wild-type bovine or human α-LA (*12*, *17*), Asp116 and Glu121 near the C-terminal 3_{10} helix show high protection factors in the BLAELZ molecule (Figure 3). Higher levels of protection are also observed for the amide protons in the antiparallel β-sheet and A- and B-helices of BLAELZ than were observed previously for bovine α-LA (*12*). Moreover, the substitution results in increases of protection factors around the loop region between the B-helix and antiparallel β-sheet (Figure 3); bovine α-LA has no residue showing a protection factor around the same region. Previous study of the hydrogen exchange behavior of ELZ has shown that the B-helix and the loop between the B-helix and β-sheet exhibit remarkable protection factors (*16*). High protection from hydrogen exchange is observed for the $N^{\epsilon 1}$ protons of three Trp residues, Trp26, 104, and 107, in BLAELZ (Table 2). Furthermore, we observed NOE cross-peaks between side chain protons (H^{β} and H^{γ}) of Val21 and $N^{\epsilon 1}$ protons of Trp26 and Trp107 (Figure 5); this observation suggests that the B-helix comes in close proximity with the introduced D-helix (Figure 6). Three Trp residues and Val21 in BLAELZ correspond to Trp28, 108, 111, and Tyr23 in ELZ, which are buried in the interior of the ELZ molecule and form a rigid hydrophobic core (*15*, *16*). Therefore, the overall structural stabilization of α-LA caused by the D-helix of ELZ may be due to structural interactions of the inserted D-helix with the B-helix (Figures 3 and 5 and Tables 2 and 4).

Chemical shift deviations and scalar coupling constants are useful for investigating protein conformations (*40*, *42*). Coupling constants, $^3J_{HN,H\alpha}$, and chemical shift deviations of BLAELZ support the conformational similarity to bovine α-LA (*5*, *9*, *10*). As described in Results, the residues in the fluctuating loop of BLAELZ have an α-helical tendency, as judged by both chemical shift deviations and $^3J_{HN,H\alpha}$. These results suggest that the fluctuating loop of BLAELZ adopts an α-helical structure.

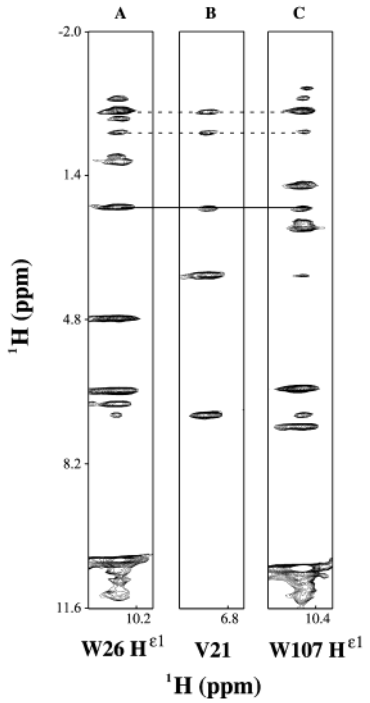

FIGURE 5: Strips taken from the 3D ^{1}H−^{15}N NOESY-HSQC (A and C) and ^{1}H−^{15}N TOCSY-HSQC (B) spectra showing the NOEs between side chain protons (H$^{\beta}$ and H$^{\gamma}$) of Val21 and side chain NH protons of Trp residues. H$^{\beta}$−H$^{\epsilon 1}$ and H$^{\gamma}$−H$^{\epsilon 1}$ NOE connectivities are shown by solid and dotted lines, respectively. A mixing time of NOESY spectrum is 100 ms.

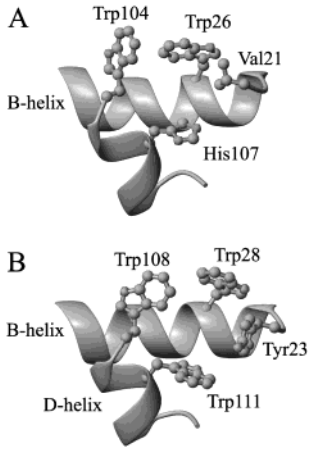

FIGURE 6: B- and D-helices of bovine α-lactalbumin (A) and equine lysozyme (B). The amino acid names and numbers are depicted. The figure was generated using the program MOLMOL (*45*).

Previous study has shown that the cross-peaks from residues Thr30, Thr33, Ser34, and His107 located in the B-helix and the fluctuating loop of bovine α-LA are much weaker than cross-peaks from residues located in other regions of the protein and that there are no cross-peaks arising from Leu105, Lys108, and Ala109 in the HSQC spectrum of bovine α-LA, since these peaks are broadened beyond detection. The broadening and/or absence of cross-peaks for the B-helix and the fluctuating loop in bovine α-LA probably reflect the dynamic structure on a millisecond to microsecond time scale (*12*). In contrast, we could observe all resonances in the B-helix and the fluctuating loop of BLAELZ in the ^{1}H−^{15}N HSQC spectrum illustrated in Figure 2. Most of the residues in the B-helix and the fluctuating loop show intense cross-peaks, and thus these regions in BLAELZ are less flexible on the millisecond to microsecond time scale than the corresponding regions in bovine α-LA. The order parameters (S^2) show that there is no significant motion on a picosecond to nanosecond time scale in the B-helix and the 105−110 region of BLAELZ (Figure 4C).

Table 5: Averaged Order Parameters of the Fluctuating Loop and Three Helices in BLAELZ

	sequence	averaged S^2
A-helix	5−11	0.934
B-helix	23−34	0.944
C-helix	86−98	0.949
fluctuating loop	105−110	0.938

We investigated the dynamics of BLAELZ by model-free analysis derived from the ^{15}N relaxation data (Figure 4). Figure 4 shows that the 105−110 region in BLAELZ has R_2 values similar to those for other structural elements in the α-domain and there is no significant R_{ex} term around the fluctuating loop. The broadening and/or absence of cross-peaks for the 105−110 region in the HSQC spectrum of bovine α-LA probably reflect conformational exchange in bovine α-LA (*12*). These results suggest that there is no conformational exchange in the 105−110 region of BLAELZ, in contrast to bovine α-LA (*43*). Therefore, our results indicate that the substitution of the fluctuating loop in bovine α-LA with the D-helix in ELZ decreases the mobility on the millisecond to microsecond time scale in the residues 105−110. Generally, the order parameters (S^2) reflect the mobility of the polypeptide on the picosecond to nanosecond time scale (*43*). The order parameters of the substituted region of BLAELZ are all higher than 0.8, suggesting rigid structure in the 105−110 region on the picosecond to nanosecond time scale. Averaged order parameters for the fluctuating loop and major α-helices are given in Table 5, indicating that the fluctuating loop is as rigid as the A-, B-, and C-helices. Averaged S^2 values of the fluctuating loop of BLAELZ are comparable with those of the D-helix in hen egg white lysozyme (*44*).

Studying the effects of amino acid substitutions on the structure and stability of a protein is useful for understanding how the protein is stabilized. Most attempts to investigate the properties of proteins have employed a single mutation or only a few mutations, which typically produce minor changes in structure. We have shown that the substitution of the fluctuating loop in bovine α-LA with the D-helix in ELZ increases the protection factors throughout the protein molecule (Figures 2 and 3). Therefore, the D-helix in ELZ affects the stability of other structural elements, and this effect is responsible for the higher stability of BLAELZ than bovine α-LA (Table 4 and Figure 5). Our results suggest that the replacement of a highly fluctuating loop in a protein with a rigid structural element in a homologous protein provides a new tool for engineering a novel protein. The use of a chimeric protein may be one of the ways to construct multifunctional and/or modified proteins.

ACKNOWLEDGMENT

We thank Dr. Shin-ichi Tate of the Japan Advanced Institute of Science and Technology (JAIST) for his valuable suggestions regarding model-free analysis.

REFERENCES

1. Khatra, B. S., Herries, D. G., and Brew, K. (1974) *Eur. J. Biochem. 44*, 537−560.
2. Bell, J. E., Beyer, T. A., and Hill, R. L. (1976) *J. Biol. Chem. 251*, 3003−3013.
3. Brew, K., Vanaman, T. C., and Hill, R. L. (1967) *J. Biol. Chem. 242*, 3747−3749.
4. Hall, L., Craig, R. K., Edbrooke, M. R., and Campbell, P. N. (1982) *Nucleic Acids Res. 10*, 3503−3515.
5. Acharya, K. R., Stuart, D. I., Walker, N. P., Lewis, M., and Phillips, D. C. (1989) *J. Mol. Biol. 208*, 99−127.
6. McKenzie, H. A., and White, F. H., Jr. (1991) *Adv. Protein Chem. 41*, 173−315.
7. Nitta, K., Tsuge, H., Sugai, S., and Shimazaki, K. (1987) *FEBS Lett. 223*, 405−408.
8. Nitta, K., and Sugai, S. (1989) *Eur. J. Biochem. 182*, 111−118.
9. Acharya, K. R., Ren, J. S., Stuart, D. I., Phillips, D. C., and Fenna, R. E. (1991) *J. Mol. Biol. 221*, 571−581.
10. Pike, A. C., Brew, K., and Acharya, K. R. (1996) *Structure 4*, 691−703.
11. Harata, K., and Muraki, M. (1992) *J. Biol. Chem. 267*, 1419−1421.
12. Forge, V., Wijesinha, R. T., Balbach, J., Brew, K., Robinson, C. V., Redfield, C., and Dobson, C. M. (1999) *J. Mol. Biol. 288*, 673−688.
13. Tsuge, H., Ago, H., Noma, M., Nitta, K., Sugai, S., and Miyano, M. (1992) *J. Biochem. 111*, 141−143.
14. Koshiba, T., Yao, M., Kobashigawa, Y., Demura, M., Nakagawa, A., Tanaka, I., Kuwajima, K., Nitta, K. (2000) *Biochemistry 39*, 3248−3257.
15. Morozova, L. A., Haynie, D. T., Arico-Muendel, C., Van Dael, H., and Dobson, C. M. (1995) *Nature Struct. Biol. 2*, 871−875.
16. Morozova-Roche, L. A., Arico-Muendel, C. C., Haynie, D. T., Emelyanenko, V. I., Van Dael, H., and Dobson, C. M. (1997) *J. Mol. Biol. 268*, 903−921.
17. Schulman, B. A., Redfield, C., Peng, Z. Y., Dobson, C. M., and Kim, P. S. (1995) *J. Mol. Biol. 253*, 651−657.
18. Kobashigawa, Y., Demura, M., Koshiba, T., Kumaki, Y., Kuwajima, K., and Nitta, K. (2000) *Proteins 40*, 579−589.
19. Mizuguchi, M., Masaki, K., and Nitta, K. (1999) *J. Mol. Biol. 292*, 1137−1148.
20. Barik, S. (1995) *Mol. Biotechnol. 3*, 1−7.
21. Peng, Z. Y., Wu, L. C., and Kim, P. S. (1995) *Biochemistry 34*, 3248−3252.
22. Rance, M., Sorensen, O. W., Bodenhausen, G., Wagner, G., Ernst, R. R., and Wüthrich, K. (1983)*Biochem. Biophys. Res. Commun. 117*, 479−485.
23. Bax, A., and Davis, D. G. (1985) *J. Magn. Reson. 65*, 353−360.
24. Griesinger, C., Otting, G., Wüthrich, K., and Ernst, R. R. (1988) *J. Am. Chem. Soc. 110*, 7870−7872.
25. Jenner, J., Meier, B. H., Bachmann, P., and Ernst, R. R. (1979) *J. Chem. Phys. 71*, 4546−4553.
26. Anli-Kumer, E., Ernst, R. R., and Wüthrich, K. (1980) *Biochem. Biophys. Res. Commun. 95*, 1−6.
27. Bax, A., Griffey, R. H., and Hawkin, B. L. (1983) *J. Magn. Reson. 55*, 301−315.
28. Kay, L. E., Marion, D., and Bax, A. (1989) *J. Magn. Reson. 84*, 72−84.
29. Vuister, G. W., and Bax, A. (1993) *J. Am. Chem. Soc. 115*, 7772−7777.
30. Delaglio, F., Grzesiek, S., Vuister, G. W., Zhu, G., Pfeifer, J., and Bax, A. (1995) *J. Biomol. NMR 6*, 277−293.
31. Bartels, C., Xia, T. H., Billeter, M., Güntert, P., and Wüthrich, K. (1995) *J. Biomol. NMR 6*, 1−10.
32. Mine, S., Tate, S., Ueda, T., Kainosho, M., and Imoto, T. (1999) *J. Mol. Biol. 286*, 1547−1565.
33. Garrett, D. S., Powers, R., Gronenborn, A. M., and Clore, G. M. (1991) *J. Magn. Reson. 95*, 214−220.
34. Palmer, A. G., Rance, M., and Wright, P. E. (1991) *J. Am. Chem. Soc. 113*, 4371−4380.
35. Mandel, A. M., Akke, M., and Palmer, A. G. (1995) *J. Mol. Biol. 246*, 144−163.
36. Marion, D., Driscoll, P. C., Kay, L. E., Wingfield, P. T., Bax, A., Gronenborn, A. M., and Clore, G. M. (1989) *Biochemistry 28*, 6150−6156.
37. Driscoll, P. C., Clore, G. M., Marion, D., Wingfield, P. T., and Gronenborn, A. M. (1990) *Biochemistry 29*, 3542−3556.
38. Kay, L. E., Keifer, P., and Saarien, T., (1992) *J. Am. Chem. Soc. 114*, 10663−10665.
39. Bai, Y., Milne, J. S., Mayne, L., and Englander, S. W. (1993) *Proteins 17*, 75−86.
40. Wishart, D. S., Sykes, B. D., and Richards, F. M. (1992) *Biochemistry 31*, 1647−1651.
41. Ishikawa, N., Chiba, T., Chen, L. T., Shimizu, A., Ikeguchi, M., and Sugai, S. (1998) *Protein Eng. 11*, 333−335.
42. Wishart, D. S., and Sykes, B. D. (1994) *J. Biomol. NMR 4*, 171−180.
43. Feher, V. A., and Cavanagh, J. (1999) *Nature 400*, 289−293.
44. Buck, M., Boyd, J., Redfield, C., MacKenzie, D. A., Jeenes, D. J., Archer, D. B., and Dobson, C. M. (1995) *Biochemistry 34*, 4041−4055.
45. Koradi, R., Billeter, M., and Wüthrich, K. (1996) *J. Mol. Graph. 14*, 51−55.

BI020360U